Identifying the influence of a large alluvial valley on train-induced vibration propagation in Rome by an integrated approach

Roberto Iannucci[1,2*], Luca Lenti[3,4], Salvatore Martino[1,2], Roberto Perazza[1], Chiara Varone[5], Francesca Bozzano[1,2]

[1] Dipartimento di Scienze della Terra, Sapienza Università di Roma, P.le A. Moro 5, 00185 Roma, Italy.
[2] Centro di Ricerca per i Rischi Geologici CERI, Sapienza Università di Roma, P.le A. Moro 5, 00185 Roma, Italy.
[3] Université Gustave Eiffel, IFSTTAR (GERS/SRO), 14-20 Boulevard Newton, Cité Descartes, Champs-sur-Marne, F-77447 Marne la Vallée Cedex 2, France.
[4] Equipe-Project MOUVGS, Centre d'Études et d'Expertise sur les Risques, l'Environnement, la Mobilité et l'Aménagement (CEREMA), 500 Route des Lucioles, Sophia-Antipolis, F-06903, France.
[5] Italian National Research Council (CNR), Institute of Environmental Geology and Geoengineering (IGAG) RM1 Via Salaria km 29.300, 00015 Montelibretti, Italy.

[*] Corresponding Author e-mail: roberto.iannucci@uniroma1.it

Keywords:

Underground train-induced vibrations; Buried alluvial valley; Engineering geological modelling; Ambient vibration analysis; FEM numerical modelling

Highlights

- Reconstruction of high-resolution engineering geological model of the Rome city centre
- On-site recording of train-induced vibrations for numerical modelling inputs
- Characterisation of the ambient vibrations in the investigated area
- 2D numerical simulation of the alluvia influence on train-induced vibrations
- Simulated vibrations propagate hundreds of meters above the regular ambient vibrations

Abstract

In recent decades, the number of tunnels has increased within city centres worldwide due to the construction of new underground train lines, thus instigating subsequent issues related to an increase in the amount of vibrations affecting pre-existing buildings and infrastructures; therefore, more studies have been devoted to investigating the interactions between underground train lines and buildings within the framework of a site-city interaction (SCI) scheme. The already designed layout of line C of the Rome Metro was chosen as the research object of a case study focusing on underground train-induced vibration propagation in the city centre of Rome (Italy). Numerical modelling was carried out to analyse the propagation of future vibrations within the large buried alluvial valley and to assess the spatial extension of the induced vibration resentment.

Two different subsoil models were considered for this study area: i) a homogeneous model (HoM), in which a homogeneous filling of Tiber alluvia was considered, and ii) a heterogeneous model (HeM), where the Tiber alluvia was distinguished within various lithotechnical units. Specific geophysical measurements were performed to i) record vibrations induced by accelerating, braking and regularly transiting trains to provide input for numerical modelling and ii) define the typical ambient vibration noise of the investigated area. Numerical modelling was then performed using the CESAR-LCPC code, which adopts a finite element method (FEM) solution in the time domain, to simulate the propagation of train-induced vibrations within the Tiber River valley in both the HoM and HeM simulations.

The simulation outputs revealed a negligible deamplification effect up to approximately 2 Hz with respect to the considered solicitation in the area located above the tunnels and a maximum effect with respect to the reference ambient vibration noise within 5 and 10 Hz along the valley. The vibrations induced by the accelerating trains can be associated with the highest resentment at the free surface of the valley. A more intense effect generally results in the HeM simulation, which highlights the nonnegligible role of the heterogeneities present within the Tiber alluvia in propagating train-induced vibrations. The numerical outputs highlight that the train-induced vibrations can propagate hundreds of metres away from the underground train location, i.e., up to 400 m astride the axis of the designed tunnels in the case study considered here, and can be distinguished with respect to the regular ambient vibration level.

1. Introduction

In recent decades, the pursuit of sustainable social and environmental development, as well as a lack of available free ground surfaces, has resulted in an increase in the use of underground tunnels within city centres worldwide in the framework of new underground train line designs (Eitzenberger 2008). As a result of the subsequent substantial rise in vibrations generated by train transit in these newly designed tunnels, the need to evaluate their propagation within subsoils, interaction with pre-existing buildings and infrastructures and perception by inhabitants has grown concurrently.

These vibrations, known as “ground-borne vibrations” (Kurzweil 1979), are generated primarily at the wheel-rail interface and then propagate into the subsoil from the tunnel to the topographical surface (Hood et al., 1996; Yang and Hsu, 2006), contributing to the ambient vibration noise of urban environments. In their propagation path, vibrations can reach nearby buildings, causing wall and flood shaking and producing ground-borne noise known as “reradiated noise” (Thompson, 2009; Connolly et al., 2016). Such shaking can induce annoyance to inhabitants, equipment malfunctions and issues with the structural stability of buildings, which are more relevant when tunnels are shallow and in close proximity to their foundations (He et al., 2018). In fact, vibrations propagating from the subsoil can induce a fatigue phenomenon in buildings as well as in their foundations, causing differential settlement, cracking, resonance-induced effects and other kinds of structural damage (Kedia and Kumar 2019).

From this perspective, the impact of newly designed underground train lines in city centres needs to be evaluated prior to installation to avoid potential damages and stability issues with above buildings due to the vibrations originating from train transit. In this regard, several numerical and analytical models have been recently developed with the aim of predicting the vibrations induced by underground railways and their propagation within the subsoil (e.g., Jones et al., 2011; Yaseri et al., 2014; Amado-Mendes et al., 2015; Xu et al., 2015; Yang et al., 2017; Zhou et al., 2017; He et al., 2018; Pan et al., 2018; Jin et al., 2020). In general, the abovementioned studies simulated vibration propagation within a homogeneous half-space, excluding that of He et al. (2018), who applied a multilayered half-space and noted that vertical variations in the subsoil can influence the propagation of train vibrations. In addition, other studies (Lopes et al., 2016; Ma et al., 2016; Zhang et al., 2021) analysed the experimental data of train vibrations recorded on site, thus supporting the need to calibrate numerical approaches with field data. In light of this, the accurate reconstruction of the subsoil geology, including its vertical and horizontal heterogeneities, as well as the use of vibrational field data, seem to be key requirements for obtaining reliable simulations of underground train-induced vibrations.

Among the geophysical investigation techniques, in the last years ambient vibration analysis approaches have been largely used for different aims, such as characterising the main features and monitoring the health state of structures and buildings (e.g., Farrar and James, 1997; Brownjohn, 2003; Gentile and Saisi, 2007; Michel et al., 2008; Shi et al., 2012), defining the main features of the shallow subsoil of a site (e.g., Bonnefoy-Claudet et al., 2006; Del Monaco et al., 2013; Pastén et al., 2016; Paolucci et al., 2017; Mascandola et al., 2019; Wang et al., 2020), obtaining information of the Earth structure (e.g., Shapiro and Campillo, 2004; Bensen et al., 2008; Stehly et al., 2009; Li et al., 2010), monitoring volcano activities (e.g., De Plaen et al., 2014; Yates et al., 2019; Qian and Liu, 2020), characterising and monitoring slopes involved by landslide processes (e.g., Burjánek et al., 2010; Del Gaudio et al., 2014, 2018; Kleinbrod et al., 2019; Iannucci et al., 2020; Kakhki et al., 2020; Martino et al., 2020).

Ambient vibration wavefield, also known as seismic ambient noise, includes ground vibrations produced by random and uncontrolled sources, natural or related to human activities, e.g., tides, sea waves striking the coasts, wind turbulences and their effects on trees or buildings, industrial machineries, road traffic, trains, etc. Several studies (Gutenberg, 1958; Asten, 1978; Asten and Henstridge, 1984; Yamanaka et al., 1993) investigated the relation between the type of source and the frequency content of seismic ambient noise, observing that usually vibrations related to natural sources (called "microseisms") have typical frequency content lower than 1 Hz and human activities produce vibrations (called "microtremors") with frequency content higher than 1 Hz, except for local wind turbulences that contribute to frequencies higher than 15-20 Hz (Bungum et al., 1985; Young et al., 1996). Ambient vibration noise related to natural sources is characterised by seasonal variations and generally results higher in winter with respect to summer (Given, 1990; McNamara and Buland, 2004). On the contrary, ambient vibration noise produced by human activities, known as anthropogenic or cultural noise, presents daily variations with higher levels during daytime with respect to nighttime (Given, 1990; McNamara and Buland, 2004; Panou et al., 2005; Groos and Ritter, 2009; Hong et al., 2020) and results higher in urban centres than rural areas (McNamara and Buland, 2004; Albert and Decato, 2017; Hong et al., 2020). The main anthropic contribution to the ambient vibration noise higher than 1 Hz is testified also by its considerable drop in urban environments during periods with reduced human activities, such as weekends (Yamanaka et al., 1993; Groos and Ritter, 2009), holidays (Groos and Ritter, 2009; Poli et al., 2020; Diaz et al., 2021; Roy et al., 2021) or the 2020 local lockdowns due to the COVID-19 pandemic (Lecocq et al., 2020; Poli et al., 2020; Diaz et al., 2021; Roy et al., 2021).

This paper proposes the results of an integrated engineering geological, geophysical and numerical approach applied to study the propagation of underground train-induced vibrations in the subsoil of the Rome city centre. Specific ambient vibration measurements were performed to record vibrations induced by transiting trains to provide a reliable input for numerical modelling and define the typical ambient vibration noise of the investigated site for comparison with the modelling outputs. A 2D numerical approach was chosen to reliably simulate vibration propagations within an alluvial valley, as testified by the large body literature regarding earthquake propagation (e.g., Gaudiosi et al., 2014; El Haber et al., 2019; Khanbabazadeh et al., 2019; Macerola et al., 2019; Ruan et al., 2019; Pergalani et al., 2020). In fact, a simulation of cross-sections with a direction perpendicular to the axis of the valley enabled to take into account its vertical and horizontal heterogeneity without the computational weight of 3D modelling.

The study area is located in the Prati neighbourhood on the right bank of the Tiber River, where line A of the Rome Metro is currently active. Within the next year, this area will also be of interest due to the completion of transit line C, a new urban train line whose construction is currently only partially completed. Considering the presence of several historical buildings in the investigated area that are exposed to underground train-induced vibrations as well as the complex subsoil setting, numerical modelling of the propagation of the induced vibrations related to future train transits was carried out.

2. Engineering geological modelling

An additional underground train line of the Rome Metro, referred to as line C, is currently under construction under the city of Rome to improve its local public transport network by connecting the city centre with suburban areas located in the eastern zone of the city. The first track of this line was operational in December 2013 and ran from the eastern suburbs to the city centre of Rome. The second track will consist of two tunnels excavated in the subsoil from the city centre towards the western suburbs and will pass through the Prati neighbourhood, where there will likely be a connection between the already existing line A and the designed line C at the Ottaviano station (www.metrocspa.it/lopera) that represents the zone considered for the present study. At present, the construction site is located on the left bank of the Tiber River.

The city centre of Rome is characterised by a complex geological and geomorphological setting due to the structural evolution of the Tyrrhenian margin (Funiciello and Giordano, 2008). Tectonic, volcanic and glacio-eustatic activities have determined the actual landscape of the city, which is characterised by hills composed of Plio-Pleistocene marine (Conato et al., 1980) and volcanic (Alvarez et al., 1996) deposits and alluvial valleys filled by post-würmian soft sediments (Marra et al., 2008).

In the historical centre of Rome, four main geological formations are outcropping (Fig. 1):

- Plio-Pleistocene marine sediments (Marne Vaticane and Monte Mario Formations) that represent the regional geological bedrock (Marra, 1993);
- volcanic deposits of the Alban Hills, which include Middle-Upper Pleistocene volcanic products that are part of the District Roman Comagmatic Province, according to Washington (1906), exhibiting compositions from K-foidite to tephrite and phonolitic tephrite (Marra et al., 2009; Freda et al., 2006; Giordano et al., 2006);
- Pre-Würmian fluvio-palustrine deposits (i.e., Santa Cecilia, Valle Giulia, San Paolo, Aurelia and Vitinia Formations) (Karner et al., 1998);
- recent alluvial deposits of the Tiber River, which consist of post-würmian soft sediments filling würmian incisions (Marra et al., 2013).

The two following units can be distinguished within the Marne Vaticane Formation:

- MV: high consistency grey and blue-grey silty and sandy deposits;
- SMV: upper portion of the MV (up to 10 m of thickness), affected by a softening process in the Later Pliocene (Bozzano et al., 2006).

According to previous studies (Bozzano et al., 2000, 2008; Martino et al., 2015), the following lithotechnical units can be distinguished within the alluvial deposits of the Tiber River in the city centre of Rome:

- G: coarse grain deposits, mainly limestone gravel in a grey, sandy-silty matrix;
- D1: grey sands and silty sands with a grey colour;
- D2: grey silty-clay sands and sandy-clay;
- C: grey clay and silty clay with a variable peaty content that gives a black colour;
- B: brown to yellow sandy and silty-sandy sediments;
- A1: green-grey silty sand and silty clay;
- A2: clay and clayey silty bands characterised by a hazel colour;
- R: anthropic filling material.

The Marne Vaticane Formation represents the local geological bedrock (Bozzano et al., 2008), while, according to the Italian Building code (NTC 2018), the top of the MV unit corresponds to a seismic bedrock, as its shear-wave value is higher than 800 m/s (Caserta et al., 2013; Pagliaroli et al., 2014; Bozzano et al., 2016, 2017; Meza-Fajardo et al., 2019). Recently, deep bedrock responsible for the presence of a very-lowfrequency resonance (0.2-0.4 Hz) range was identified in the Rome city centre by geophysical surveys (Marcucci et al., 2019).

In this study, two subsoil models were considered along the AA' geological cross-section, depicted in Figure 1, following the approach used in previous studies (Bozzano et al., 2008; Bourdeau et al., 2019; Pergalani et al., 2020); in the first homogeneous model (HoM), the Tiber River alluvia and SMV were considered homogeneous deposits, while in the second heterogeneous model (HeM), they were distinguished in lithotechnical units (Fig. 2) according to the high-resolution engineering geological model proposed by Bozzano et al. (2000, 2008). This model was reconstructed on the basis of several tens of borehole logs, geophysical and geotechnical in situ surveys as well as laboratory tests aimed at obtaining physics parameters and static and dynamic behaviour characterisation of the alluvial deposits of the Tiber River valley. Numerical modelling was carried out for both subsoil models to evaluate the role played by the lateral and horizontal heterogeneities of alluvial plain filling with respect to the induced vibrations and their maximum resentment along the free surface.

3. Vibration data acquisition and processing

Geophysical measurements were collected during 2018 in two different neighbourhoods of Rome to record both the i) vibrations induced by the train transits, with the aim of recording signals to be subsequently used as inputs for numerical modelling of the vibration propagation, and the ii) ambient noise representative of the typical vibrational field in the neighbourhood of interest in the absence of train traffic to be compared with the values obtained in the numerical modelling forced by the input from train transits.

3.1. Train transit vibration recording

On 17 May 2018, the first geophysical acquisition campaign was performed to record vibrations generated by train transit. The records were collected at the free surface next to the tracks of line B and the Roma-Lido urban railway in proximity to the Marconi station (Fig. 3a), where both lines transit at the ground level. This site was chosen due to the outcropping of the Alban Hill volcanic deposits (Funiciello et al. 2008; Funiciello and Giordano 2008), that act as seismic bedrock, with the aim of recording train-induced vibrations and avoiding any local site amplification effects. These measurements were not performed in the Prati neighbourhood for two reasons: i) the path of line A is in tunnel and it is not possible to install sensors next to its tracks; i) the path of line A is within the valley filling, so it is not possible to exclude local amplification effects on the recorded signals.

The recording device consisted of an LE-3Dlite MkIII three-component seismometer (1 Hz eigenmode) produced by Lennartz Electronic GmbH, coupled with a REFTEK 130-01 datalogger with a sampling rate of 500 Hz (Fig. 3b). Four railway tracks related to the two different lines are present in the acquisition area; line B trains stops at the Marconi station and the Roma-Lido urban railway trains that do not stop at this station. In light of this, three different types of train signals were recorded: i) line B trains as they accelerate after leaving the Marconi station; ii) line B trains as they brake to stop at the Marconi station; and iii) Roma-Lido trains regularly transiting as they do not stop at the Marconi station.

Since tens of train transits were recorded during the field campaign, one single signal was chosen to represent each type of train transit based on the quality of the recording, i.e., no overlap with other train transits or other vibration sources and a clear start and stop of the train transit recording. After this selection, several computations were carried out on the selected signals using the Seismic Analysis Code (SAC) (Goldstein et al., 2003). The NS and EW horizontal components of the train transit were projected to obtain the parallel (y) and perpendicular (x) motion components with respect to the railway tracks. A multiplicative factor was then applied to each time history to correct the signals, which theoretically reports their values at the railway track, according to the amplitude decremental law (Eq. 1) proposed by Jamal-Eddine et al. (2018):

$$k = 1.6034\ d^{-0.884} \qquad (1)$$

where k is a corrective factor for the signal amplitude and d is the distance between the trainway track and the recording sensor.

The fast Fourier transform (FFT) computed for each time history reported that the energy of the train transit is concentrated in the frequency range 1-60 Hz and has a frequency peak between 6 and 8 Hz with a frequency content peak value that tends to increase as the speed of the train increased, i.e., passing from the breaking trains (lower values) to the accelerating trains (higher values). Such frequency content values are compatible with urban and non-high-speed trains (Ju et al., 2009; Milne et al., 2017). The regularly transiting train signals present a frequency content at about 1 Hz higher than the other two train types that seems to be a specific feature of this train transit type. The selected time histories were processed by: i) bandpass filtering in the frequency range 1-60 Hz (i.e., in which the energy of the train transit is focused); ii) interpolation with a sampling rate of 200 Hz; and iii) integration to obtain the displacement signals. In this way, displacement time histories representative of the accelerating, braking and regularly transiting trains were obtained for numerical modelling (Fig. 4).

3.2. Ambient vibration measurements

On 5 October 2018, a second geophysical campaign was performed to measure the ambient vibration noise in the Prati neighbourhood, corresponding to the planned location of the intersection of the future line C at cross-section AA', as shown in Figure 1. The measurements allowed to derive i) the horizontal and vertical mean levels of ambient vibration noise and ii) the horizontal and vertical mean amplitude spectra of the ambient vibration noise.

One-hour ambient noise records were collected at 6 measurement points by the previously described devices with the aforementioned settings; measurements were carried out on a workday during the daytime to provide the typical maximum ambient vibration level occurring in the investigated area.

The time histories of the ambient vibration records were processed by the SAC as those containing the train transits: i) the NS and EW horizontal components were composed to allow the rotating signal to be parallelly (y) and perpendicularly (x) oriented with respect to the AA' cross-section of Figure 1; ii) a bandpass filter was applied in the frequency range 1-60 Hz; and iii) an interpolation process was performed with a 200 Hz sampling rate. The arithmetic mean of signal amplitude was computed for each time history, and these values were then averaged to obtain the horizontal and vertical amplitude signal mean values of the ambient vibration noise for the study area, which were equal to 3.50E-06 m/s and 7.19E-06 m/s, respectively.

The horizontal and vertical mean FFT amplitude spectra were also obtained using Geopsy software (Wathelet et al., 2020) by i) dividing the recorded time histories into 20-s nonoverlapping windows with 5% cosine taper; ii) computing the FFT for each time history window with the Konno and Ohmachi (1998) smoothing function; and iii) averaging the obtained horizontal and vertical FFT amplitude spectra.

4. Numerical modelling

The 2D numerical modelling was performed using the CESAR-LCPC code (Humbert et al., 2005), which adopts a finite element method (FEM) solution in the time domain. The modelling considered the future locations of the train tunnels, according to the present project of line C of the Rome Metro (www.metrocspa.it). The HoM (Fig. 2) is characterised by a buried alluvial valley filled with clay and peaty clay deposits (C unit) overlying the seismic bedrock (MV). The C unit was chosen because it is the thickest and most widespread of the recent Tiber River deposits. In contrast, in the HeM (Fig. 2), the valley is filled by all lithotechnical units that composed the recent Tiber River deposits. The properties assigned to these materials (Tab. 1) were derived from Bozzano et al. (2000, 2008) and Martino et al. (2015). In addition, an equivalent material representative of the ballast of the railway track was simulated at the base of the tunnels.

A viscoelastic behaviour is assumed considering a Rayleigh-type damping according to Eq. (2):

$$[C] = \alpha.[K] + \beta.[M] \qquad (2)$$

where $[K]$ and $[M]$ are stiffness and mass matrices and α and β are Rayleigh constants that define the frequency dependence of the damping ratio. The damping percentage and related Rayleigh constants assigned to each material are also reported in Table 1. The damping quality factor Q (Table 1) was calculated by a Generalized Maxwell model through the relation proposed by Semblat (1997) for materials characterised by moderate values of damping coefficient.

The numerical domain was generated by a three-node mesh whose resolution was calibrated on the minimum wavelength in the models to reduce numerical dispersion resulting from the coarse mesh. Triangular elements of 0.5 m for the alluvial filling and 4.5 m for the seismic bedrock were selected. A set of heterogeneous absorbing layers based on the Rayleigh/Caughey damping formulation (CALM) was simulated at the lateral and bottom boundaries of the domain (Semblat et al., 2011) to avoid spurious wave reflection at the model boundaries. The CALM was composed of 5 layers with a damping variable value ranging from Qmin-1 ≈ 0.20, or $\xi = 0.10$ (in the inner part of the model), to Qmin-1 ≈ 2.00, or $\xi = 1.00$ (at the external lateral and bottom boundaries of the model). This solution guaranteed the maximum efficiency of the CALM for the heterogeneous alluvial domain (Varone et al., 2019, 2021). The model was forced by the train transit recordings (Fig. 4) and applied as vertical displacement at the base of the left railway tunnel. The vector of imposed vertical displacement as function of time was applied at the nodal elements composing the base of the tunnel and propagated as in-plane displacement.

Figures 6 and 7 show the obtained displacement time histories along the HoM and HeM model surface using wave propagation maps (WPMs). The WPMs highlight that the vibrations propagate symmetrically across the tunnel axis; the propagation distance is the same for both the vertical and horizontal components of ground motion and for all three considered inputs, even if for the HoM it is shorter when compared with the HeM. The horizontal component appears to be characterised by a spatial shift towards the northwest relative to the vertical component for both models, even if it is greater for the HeM (Fig. 7) than the HoM (Fig. 6).

Regarding the ground motion amplitude of the vibrations induced by a given type of train transit, the horizontal component is characterised by higher amplitude values with respect to the vertical component for both models. The FFT spectral ratio between the ground motion on the free surface of the numerical domain (output) and the train transit recordings (input) was computed to assess the variations in the frequential content of the signal motion when propagating within the soft alluvial soils (Figs. 8 and 9). The ground motion at the model free surface reveals a deamplification pattern showing an exponential trend with respect to the distance from the axis of the underground track that is more notable for the HeM. The outputs at the free surface over the tunnels present negligible deamplification (i.e., output/input spectral ratio equal to 0.8-1.0) up to approximately 2 Hz for all three train transit records and for both models. There are no relevant changes in terms of the deamplification effect when considering the various inputs from the different train transit types. Such deamplification could be associated with a “shadow effect”, whereby the highest response level is usually found at a certain distance from the underground tunnel and not in the zone just above it, as evidenced by the experimental and numerical data reported by Jin et al. (2020).

To deeper understanding the role of the different layers on the response of the alluvial valley to train vibrations, the transfer function at different depths within the soil overlaying the underground track were computed for the HeM outputs (Fig. 9). FFT spectral ratios reveals that the negligible deamplification at approximately 2 Hz is constantly present at different depths, just like the frequency peak at 10 Hz. The first frequency could represent the fundamental frequency of the valley while the second one is due to the frequential content of the signal motion. A frequency peak at approximately 20 Hz appears starting from -5 m from ground surface (Fig. 9) and it is due to anthropic filling material (R unit). The peak around 6 Hz is ascribable to the combined effect of units R and A1-A2 characterising the upper portion of the alluvial valley filling.

5. Discussion

Figure 10 shows the spatial distribution of the FFT spectral ratio between the modelled ground motion at the free surface (output) and the ambient vibration noise of the investigated site. The propagation of train vibrations along the cross-section supports a resentment distance above the reference ambient vibration level within the range 1000-1200 m for the accelerating train and 800-1000 m for the braking and regularly transiting trains in the frequency range between 5 and 10 Hz; the distance of the resentment progressively decreases with increasing frequency in all three train cases. It is also possible to observe that the vibrations from the accelerating trains present significantly larger FFT amplitude spectral values than those of the braking and regularly transiting trains; as a consequence, the output/noise spectral ratio reaches 900 for the accelerating train and up to 30 for the braking and regularly transiting trains.

In Figure 11, the results output by the HoM and HeM simulations are compared in terms of the mean velocity distribution of each time history obtained on the ground surface along cross-section AA' in Figure 1; the mean level of ambient vibration noise for the investigated area is also shown. The highest mean velocity values for the different train transit simulations are not generally found just above the tunnels, confirming the presence of the "shadow effect". For both models, the accelerating train phase presents mean velocity values that are higher than the mean ambient vibration level for the whole length of the cross-section. Conversely, the amplitude values of the regularly transiting and braking trains are higher than that of the ambient vibrations at a distance from the tunnels of approximately 500 m in the HoM case and 800 m in the HeM case. This difference is due to the rheological behaviour of Unit C composing the HoM. Its high damping ratio (ξ= 3% at strain 0.001%) determines a higher attenuation of the vibration and the ground motion is completely damped in a shorter distance. Additionally, the signal from the accelerating train modelled in the HeM simulation is higher than that in the HoM simulation. Such an intense vibrational effect in the HeM simulation can be attributed to the presence of a unit B level composed of sandy and silty-sandy sediments that likely responds to train vibrations with a lower attenuation and favours their propagation within the alluvial valley. A validation of the results here presented could be performed by carrying out ambient vibration measurements when line C will be operative in the investigated area and comparing the ambient noise in pre- and post-metro transit conditions.

As a final remark, despite the nature of the considered input (vertical displacement on the railway embankment), the horizontal component of the surface ground vibration is not negligible and can be higher than that of the vertical component (e.g., for regularly transiting trains in Figure 10). This effect results from the transformation of vertical energy given by the railway embankment into surface wave energy (Kawase and Aki, 1989; Hatayama et al., 1995; Meza-Fajardo et al., 2015, 2019) that generates both vertical and horizontal motions above all for the HeM case (Figs. 10 and 11).

6. Conclusions

Vibrations induced by underground trains in a large buried alluvial valley were analysed here through a numerical approach considering the Rome city centre. The modelling results reveal a general deamplification effect of the ground motion considered at the free surface with respect to the input. This effect decreases with increasing distance across the tunnel axis following an exponential trend, excluding the area located above the tunnels, where the deamplification effect is negligible, i.e., up to approximately 2 Hz in the case of the Tiber River valley in Rome for the three considered inputs.

The vibrations generated by the accelerating train transit cause a more intense effect with respect to the other two conditions in both the HoM and HeM simulations; moreover, the intensity of the induced vibrations is significantly higher than that for the ambient vibration noise both in terms of the FFT spectral amplitude and the mean velocity values.

More intense vibrational effects are obtained in the HeM relative to the HoM for each considered input; such an effect is likely associated with the rheological behaviour of the lithological units. The sandy and silty-sandy level of the HeM produces a lower attenuation of the vibrations emitted by the transiting trains, and their propagation within the alluvial filling of the valley is favoured. Conversely, grey clay and silty clay with a variable peaty level in HoM determines a higher attenuation of the vibration and the ground motion is completely damped in a shorter distance. Such effects are clearly showed even though the limitations due to the two-dimensional assumption for soil attenuation in numerical modelling.

In the light of the obtained results, the output differences in terms of waves propagations between the HoM and HeM highlight the importance of making the effort to reconstruct a complex engineering geological model that best reflect the subsoil characteristics of the investigated site. The research presented here represents a starting contribution to study any possible interactions between buildings and underground train-induced vibrations within the framework of a more complex site-city interaction (SCI) scheme devoted to reducing structural vulnerability and damages due to recurrent anthropogenic vibrations in urban areas.

Acknowledgements

This research was carried out in the framework of the Italian National project "URGENT - Urban Geology and Geohazards: Engineering geology for safer, resilieNt and smart ciTies" (PRIN2017 - Prot. 2017HPJLPW. Responsible for Sapienza University of Rome: F. Bozzano).

The activities of C. Varone were partly carried out when she was a lecturer at École Supérieure d'Ingénieurs des Travaux de la Construction (ESITC) of Paris (France) and a researcher associated with IFSTTAR GERS-SV of Marne-la-Vallée (France).

The authors wish to thank the ESITC and the IFSTTAR of Paris for hosting R. Perazza during the staging periods. The authors are grateful to the owners and the staff of the restaurant Lo Convento, who allowed vibration recording. Finally, the authors wish to thank the four anonymous reviewers whose useful and constructive suggestions made possible to improve the original manuscript.

In the present study: R. Perazza contributed to the engineering geological modelling, geophysical investigations and numerical modelling within the framework of his master's thesis; F. Bozzano and S. Martino performed engineering geological modelling; R. Iannucci carried out vibrational data acquisition and processing; L. Lenti and C. Varone performed numerical modelling; S. Martino was responsible for the scientific study design and coordinated the research; and all the authors contributed to writing the manuscript.

References

Albert, D.G., Decato, S.N., 2017. Acoustic and seismic ambient noise measurements in urban and rural areas. Appl. Acoust., 119, 135-143.

Alvarez, W., Ammerman, A.J., Renne, P.R., Karner, D.B., Terrenato, N., Montanari, A., 1996. Quaternary fluvial-volcanic stratigraphy and geochronology of the Capitoline hill in Rome. Geology, 24, 751-754.

Amado-Mendes, P., Costa, P.A., Godinho, L.M., Lopes, P., 2015. 2.5 D MFS–FEM model for the prediction of vibrations due to underground railway traffic. Eng. Struct., 104, 141-154.

Asten, M.W., 1978. Geological control of the three-component spectra of Rayleigh-wave microseisms. Bull. Seism. Soc. Am., 68(6), 1623-1636.

Asten, M.W., Henstridge, J.D., 1984. Arrays estimators and the use of microseisms for reconnaissance of sedimentary basins. Geophysics, 49(11), 1828-1837.

Bensen, G.D., Ritzwoller, M.H., Shapiro, N.M., 2008. Broadband ambient noise surface wave tomography across the United States. J. Geophys. Res. Solid Earth, 113(B5), B05306.

Bonnefoy-Claudet, S., Cornou, C., Bard, P.Y., Cotton, F., Moczo, P., Kristek, J., Fäh, D. 2006. H/V ratio: a tool for site effects evaluation. Results from 1-D noise simulations. Geophys. J. Int., 167(2), 827-837.

Bourdeau, C., Lenti, L., Cercato, M., Hailemikael, S., Martino, S., Varone, C., 2019. Numerical modelling of local seismic response in alluvial valleys filled by heterogeneous deposits for seismic microzonation studies in northern Latium (Italy), in Earthquake Geotechnical Engineering for Protection and Development of Environment and Constructions. Proceedings of the 7th International Conference on Earthquake Geotechnical Engineering, pp 1519-1526, eds Silvestri, F., Moraci, N., CRC Press/Balkema, Leiden (NL).

Bozzano, F., Andreucci, A., Gaeta, M., Salucci, R., 2000. A geological model of the buried Tiber River Valley beneath the historical centre of Rome. Bull. Eng. Geol. Environ., 58, 1-22.

Bozzano, F., Martino, S., Priori, M., 2006. Natural and man-induced stress evolution of slopes: The Monte Mario Hill in Rome. Environ. Geol., 50(4), 505-524.

Bozzano, F., Caserta, A., Govoni, A., Marra, F., Martino, S., 2008. Static and dynamic characterization of alluvial deposits in the Tiber River Valley: New data for assessing potential ground motion in the City of Rome. J. Geophys. Res. Solid Earth, 113, B01303.

Bozzano, F., Lenti, L., Marra, F., Martino, S., Paciello, A., Scarascia Mugnozza, G., Varone, C., 2016. Seismic response of the geologically complex alluvial valley at the "Europarco Business Park" (Rome – Italy) through instrumental records and numerical modelling. Ital. J. Eng. Geol. Environ., 16(1), 37-55.

Bozzano, F., Buccellato, A., Coletti, F., Martino, S., Marra, F., Rivellino, S., Varone, C., 2017. Analysis of the seismic site effects along the ancient Via Laurentina (Rome). Ann. Geophys., 60(4), S0435.

Brownjohn, J.M., 2003. Ambient vibration studies for system identification of tall buildings. Earthq. Eng. Struct. Dyn., 32(1), 71-95.

Bungum, H., Mykkeltveit, S., Kvaerna, T., 1985. Seismic noise in Fennoscandia, with emphasis on high frequencies. Bull. Seism. Soc. Am., 75(6), 1489-1513.

Burjánek, J., Gassner-Stamm, G., Poggi, V., Moore, J.R., Fäh, D., 2010. Ambient vibration analysis of an unstable mountain slope. Geophys. J. Int., 180(2), 820-828.

Caserta, A, Boore, D.M., Rovelli, A., Govoni, A., Marra, F., Della Monica, G., Boschi, E., 2013. Ground Motions Recorded in Rome during the April 2009 L'Aquila Seismic Sequence: Site Response and Comparison with Ground-Motion Predictions Based on a Global Dataset. Bull. Seismol. Soc. Am., 103(3), 1860-1874.

Conato, V., Esu, D., Malatesta, A., Zarlenga, F., 1980. New data on the Pleistocene of Rome. Quaternaria, 22, 131-176.

Connolly, D.P., Marecki, G.P., Kouroussis, G., Thalassinakis, I., Woodward, P.K., 2016. The growth of railway ground vibration problems—A review. Sci. Total Environ. 568, 1276-1282.

De Plaen, R.S., Lecocq, T., Caudron, C., Ferrazzini, V., Francis, O., 2016. Single-station monitoring of volcanoes using seismic ambient noise. Geophys. Res. Lett., 43(16), 8511-8518.

Del Gaudio, V., Muscillo, S., Wasowski, J., 2014. What we can learn about slope response to earthquakes from ambient noise analysis: an overview. Eng. Geol., 182, 182-200.

Del Gaudio, V., Luo, Y., Wang, Y., Wasowski, J., 2018. Using ambient noise to characterise seismic slope response: the case of Qiaozhuang peri-urban hillslopes (Sichuan, China). Eng. Geol., 246, 374-390.

Del Monaco, F., Tallini, M., De Rose, C., Durante, F., 2013. HVNSR survey in historical downtown L'Aquila (central Italy): Site resonance properties vs. subsoil model. Eng. Geol., 158, 34-47.

Diaz, J., Ruiz, M., Jara, J.A., 2021. Seismic monitoring of urban activity in Barcelona during the COVID-19 lockdown. Solid Earth, 12(3), 725-739.

Eitzenberger, A., 2008. Train-induced vibrations in tunnels: a review. Luleå tekniska universitet, Luleå (SE).

El Haber, E., Cornou, C., Jongmans, D., Youssef Abdelmassih, D., Lopez-Caballero, F., Al Bitter, T., 2019. Influence of 2D heterogeneous elastic soil properties on surface ground motion spatial variability. Soil Dyn. Earthq. Eng., 123, 75-90.

Farrar, C.R., James, G.H., 1997. System identification from ambient vibration measurements on a bridge. J. Sound Vib., 205(1), 1-18.

Freda, C., Gaeta, M., Karner, D.B., Marra, F., Renne, P.R., Taddeucci, J., Scarlato, P., Christensen, J.N., Dallai, L., 2006. Eruptive history and petrologic evolution of the Albano multiple maar (Alban Hills, Central Italy). Bull. Volcanol., 68, 567-591.

Funiciello, R., Barisone, G., Cipollari, P., Di Bella, L., Faranda, C., Gliozzi, E., Lo Mastro, S., Corazza, A., Cruciani, D., Esposito, A., Manzon, V., Valentino, A., Fabbri, M., Giordano, G., Marsili, P., Mazzini, I., Paccara, P., Pieruccini, P., Rodani, S., Rosa, C., Cecili, A., Felici, M., Gini, R., 2008. Carta geologica d'Italia alla scala 1:50.000. Foglio 374 Roma. APAT, Dipartimento Difesa del Suolo, Servizio Geologico d'Italia, S.EL.CA., Firenze (IT).

Funiciello, R., Giordano, G., 2008. Note illustrative carta geologica d'Italia alla scala 1:50.000. Foglio 374 Roma. APAT, Dipartimento Difesa del Suolo, Servizio Geologico d'Italia, S.EL.CA., Firenze (IT).

Gaudiosi, I., Del Monaco, F., Milana, G., Tallini, M., 2014. Site effects in the Aterno River Valley (L'Aquila, Italy): comparison between empirical and 2D numerical modelling starting from April 6th 2009 Mw 6.3 earthquake. Bull. Earthq. Eng., 12(2), 697-716.

Gentile, C., Saisi, A., 2007. Ambient vibration testing of historic masonry towers for structural identification and damage assessment. Constr. Build. Mater., 21(6), 1311-1321.

Giordano, G., De Benedetti, A.A., Diana, A., Diano, G., Gaudioso, F., Marasco, F., Micelli, M., Mollo, S., Cas, R.A.F., Funiciello, R., 2006. The Colli Albani caldera (Roma, Italy): Stratigraphy, structure and petrology. J. Volcanol. Geotherm. Res., 155(1-2), 49-80.

Given, H.K., 1990. Variations in broadband seismic noise at IRIS/IDA stations in the USSR with implications for event detection. Bull. Seismol. Soc. Am., 80(6B), 2072-2088.

Goldstein, P., Dodge, D., Firpo, M., Lee, M., 2003. SAC2000: Signal processing and analysis tools for seismologists and engineers, in The IASPEI International Handbook of Earthquake and Engineering Seismology, vol 81, pp 1613-1620, eds Lee, W.H.K., Kanamori, H., Jennings, P.C., Kisslinger, C., Academic Press, London (GB).

Groos, J.C., Ritter, J.R.R., 2009. Time domain classification and quantification of seismic noise in an urban environment. Geophys. J. Int., 179(2), 1213-1231.

Gutenberg, B., 1958. Microseisms. Adv. Geophys., 5, 53-92.

Hatayama, K., Matsunami, K., Iwata, T., Irikura, K., 1995. Basin-induced love waves in the eastern part of the Osaka Basin. Journal of Physics of the Earth, 43(2), 131-55.

He, C., Zhou, S., Di, H., Guo, P., Xiao, J., 2018. Analytical method for calculation of ground vibration from a tunnel embedded in a multi-layered half-space. Comput. Geotech., 99, 149-164.

Hong, T.K., Lee, J., Lee, G., Lee, J., Park, S., 2020. Correlation between ambient seismic noises and economic growth. Seismol. Res. Lett., 91(4), 2343-2354.

Hood, R.A., Greer, R.J., Breslin, M., Williams, P.R., 1996. The calculation and assessment of ground-borne noise and perceptible vibration from trains in tunnels. J. Sound Vib., 193(1), 215-225.

Humbert, P., Fezans, G., Dubouchet, A., Remaund, D., 2005. CESAR-LCPC: a computing software package dedicated to civil engineering uses. Bullettin des Laboratoires des Ponts et Chaussée, 256/257, 7-37.

Iannucci, R., Martino, S., Paciello, A., D'Amico, S., Galea, P., 2020. Investigation of cliff instability at Għajn Ħadid Tower (Selmun Promontory, Malta) by integrated passive seismic techniques. J. Seismol., 24, 897-916.

Jamal-Eddine, A.K., Lenti, L., Semblat, J.F., 2018. Aléa vibratoire dans les sols: indicateurs pertinents et classification simplifiée. Revue Française de Géotechnique, 155, 4.

Jin, Q., Thompson, D.J., Lurcock, D.E., Ntotsios, E., 2020. The shadow effect on the ground surface due to vibration transmission from a railway tunnel. Transp. Geotech., 23, 100335.

Jones, S., Hunt, H., 2011. Voids at the tunnel–soil interface for calculation of ground vibration from underground railways. J. Sound Vib., 330(2), 245-270.

Ju, S.H., Lin, H.T., Huang, J.Y., 2009. Dominant frequencies of train-induced vibrations. J. Sound. Vib., 319(1-2), 247-259.

Kakhki, M.K., Peters, F.C., Mansur, W.J., SadidKhoii, A., Rezaei, S., 2020. Deciphering site response directivity in landslide-prone slopes from ambient noise spectral analysis. Eng. Geol., 269, 105542.

Karner, D.B., Marra, F., 1998. Correlation of fluvio deltaic aggradational sections with glacial climate history: a revision of the classical Pleistocene stratigraphy of Rome. Geol. Soc. Am. Bull., 110, 48-758.

Kawase, H., Aki, K., 1989. A study on the response of a soft basin for incident S, P, and Rayleigh waves with special reference to the long duration observed in Mexico city. Bull. Seismol. Soc. Am., 79(5), 1361-1382.

Kedia, N.K., Kumar, A., 2019. A review on vibration generation due to subway train and mitigation techniques, in Geotechnics for Transportation Infrastructure, pp 295-308, eds Sundaram, R., Shahu, J., Havanagi, V., Springer, Singapore (SG).

Kleinbrod, U., Burjánek, J., Fäh, D., 2019. Ambient vibration classification of unstable rock slopes: a systematic approach. Eng. Geol., 249, 198-217.

Khanbabazadeh, H., Hasal, M.E., Iyisan, R., 2019. 2D seismic response of the Duzce Basin Turkey. Soil Dyn. Earthq. Eng., 125, 105754.

Konno, K., Ohmachi, T., 1998. Ground-motion characteristics estimated from spectral ratio between horizontal and vertical components of microtremor. Bull. Seismol. Soc. Am., 88, 228-241.

Kurzweil, L.G., 1979. Ground-borne noise and vibration from underground rail systems. J. Sound Vib., 66(3), 363-370.

Li, H., Bernardi, F., Michelini, A., 2010. Surface wave dispersion measurements from ambient seismic noise analysis in Italy. Geophys. J. Int., 180(3), 1242-1252.

Lecocq, T. et al., 2020. Global quieting of high-frequency seismic noise due to COVID-19 pandemic lockdown measures. Science, 369(6509), 1338-1343.

Lopes, P., Ruiz, J.F., Costa, P.A., Rodríguez, L.M., Cardoso, A.S., 2016. Vibrations inside buildings due to subway railway traffic. Experimental validation of a comprehensive prediction model. Sci. Total Environ., 568, 1333-1343.

Ma, M., Liu, W., Qian, C., Deng, G., Li, Y., 2016. Study of the train-induced vibration impact on a historic Bell Tower above two spatially overlapping metro lines. Soil Dyn. Earthq. Eng., 81, 58-74.

Macerola, L., Tallini, M., Di Giulio, G., Nocentini, M., Milana, G., 2019. The 1-D and 2-D seismic modeling of deep quaternary basin (Downtown L'Aquila, Central Italy). Earthq. Spectra, 35(4), 1689-1710.

Marcucci, S., Milana, G., Hailemikael, S., Carlucci, G., Cara, F., Di Giulio, G., Vassallo, M., 2019. A Deep Bedrock in Rome, Italy: A new constraint based on a passive seismic data analysis. Pure Appl. Geophys., 176, 2395-2410.

Marra, F., 1993. Stratigrafia ed assetto geologico-strutturale dell'area romana tra il Tevere e il Rio Galeria. Geologica Romana, 29, 515-535.

Marra, F., Florindo, F., Boschi, E., 2008. History of glacial terminations from the Tiber River, Rome: Insights into glacial forcing mechanisms. Paleoceanography, 23(2), PA2205.

Marra, F., Karner, D.B., Freda, C., Gaeta, M., Renne, P., 2009. Large mafic eruptions at Alban Hills Volcanic District (Central Italy): Chronostratigraphy, petrography and eruptive behavior. J. Volcanol. Geotherm. Res., 179(3-4), 217-232.

Marra, F., Bozzano, F., Cinti, F.R., 2013. Chronostratigraphic and lithologic features of the Tiber River sediments (Rome, Italy): Implications on the post-glacial sea-level rise and Holocene climate. Glob. Planet Change, 107, 157-176.

Martino, S., Lenti, L., Gelis, C., Giacomi, A.C., Santisi D'Avila, P., Bonilla, F., Bozzano, F., Semblat, J.F., 2015. Influence of lateral heterogeneities on strong motion shear strains: simulations in the historical center of Rome (Italy). Bull. Seismol. Soc. Am., 105(5), 2604-2624.

Martino, S., Cercato, M., Della Seta, M., Esposito, C., Hailemikael, S., Iannucci, R., Martini, G., Paciello, A., Scarascia Mugnozza, G., Seneca, D., Troiani, F., 2020. Relevance of rock slope deformations in local seismic response and microzonation: Insights from the Accumoli case-study (central Apennines, Italy). Eng. Geol., 266, 105427.

Mascandola, C., Massa, M., Barani, S., Albarello, D., Lovati, S., Martelli, L., Poggi, V., 2019. Mapping the seismic bedrock of the Po Plain (Italy) through ambient-vibration monitoring. Bull. Seismol. Soc. Am., 109(1), 164-177.

McNamara, D.E., Buland, R.P., 2004. Ambient noise levels in the continental United States. Bull. Seismol. Soc. Am., 94(4), 1517-1527.

Meza-Fajardo, K.C., Papageorgiou, A.S., Semblat, J.F., 2015. Identification and extraction of surface waves from three-component seismograms based on the Normalized Inner Product. Bull. Seismol. Soc. Am., 105(1), 210-229.

Meza-Fajardo, K.C., Varone, C., Lenti, L., Martino, S., Semblat, J.F., 2019. Surface waves in a highly heterogeneous alluvial basin: Case study of the Fosso di Vallerano valley, Rome, Italy. Soil Dyn. Earthq. Eng., 120, 292-300.

Michel, C., Guéguen, P., Bard, P.Y., 2008. Dynamic parameters of structures extracted from ambient vibration measurements: An aid for the seismic vulnerability assessment of existing buildings in moderate seismic hazard regions. Soil Dyn. Earthq. Eng., 28(8), 593-604.

Milne, D.R.M., Le Pen, L.M., Thompson, D.J., Powrie, W., 2017. Properties of train load frequencies and their applications. J. Sound Vib., 397, 123-140.

Pagliaroli, A., Quadrio, B., Lanzo, G., Sanò, T., 2014. Numerical modelling of site effects in the Palatine Hill, Roman Forum, and Coliseum Archaeological Area. Bull. Earthq. Eng., 12, 1383-1403.

Pan, P., Shen, S., Shen, Z., Gong, R., 2018. Experimental investigation on the effectiveness of laminated rubber bearings to isolate metro generated vibration. Measurement, 122, 554-562.

Panou, A.A., Theodulidis, N.P., Hatzidimitriou, P.M., Savvaidis, A.S., Papazachos, C.B., 2005. Reliability of ambient noise horizontal-to-vertical spectral ratio in urban environments: the case of Thessaloniki City (Northern Greece). Pure Appl. Geophys., 162(5), 891-912.

Paolucci, E., Lunedei, E., Albarello, D., 2017. Application of the principal component analysis (PCA) to HVSR data aimed at the seismic characterization of earthquake prone areas. Geophys. J. Int., 211(1), 650-662.

Pastén, C., Sáez, M., Ruiz, S., Leyton, F., Salomón, J., Poli, P., 2016. Deep characterization of the Santiago Basin using HVSR and cross-correlation of ambient seismic noise. Eng. Geol., 201, 57-66.

Pergalani, F., Pagliaroli, A., Bourdeau, C., Compagnoni, M., Lenti, L., Lualdi, M., Madiai, C., Martino, S., Razzano, R., Varone, C., Verrubbi, V., 2020. Seismic microzoning map: approaches, results and applications after the 2016–2017 Central Italy seismic sequence. Bull. Earthq. Eng., 18(12), 5595-5629.

Poli, P., Boaga, J., Molinari, I., Cascone, V., Boschi, L., 2020. The 2020 coronavirus lockdown and seismic monitoring of anthropic activities in Northern Italy. Scientific Reports, 10(1), 1-8.

Qian, R., Liu, L., 2020. Imaging the active faults with ambient noise passive seismics and its application to characterize the Huangzhuang-Gaoliying fault in Beijing Area, northern China. Eng. Geol., 268, 105520.

Roy, K.S., Sharma, J., Kumar, S., Kumar, M.R., 2021. Effect of coronavirus lockdowns on the ambient seismic noise levels in Gujarat, northwest India. Scientific Reports, 11(1), 1-13.

Ruan, B., Zhao, K., Wang, S.Y., Chen, G.X., Wang, H.Y., 2019. Numerical modeling of seismic site effects in a shallow estuarine bay (Suai Bay, Shantou, China). Eng. Geol., 260, 105233.

Semblat, J.F., 1997. Rheological interpretation of Rayleigh damping. J. Sound. Vib., 206(5), 741-744.

Semblat, J.F., Lenti, L., Gandomzadeh, A., 2011. A simple multi-directional absorbing layer method to simulate elastic wave propagation in unbounded domains. Int. J. Numer. Methods Eng., 85, 1543-1563.

Shapiro, N.M., Campillo, M., 2004. Emergence of broadband Rayleigh waves from correlations of the ambient seismic noise. Geophys. Res. Lett., 31(7), L07614.

Shi, W., Shan, J., Lu, X., 2012. Modal identification of Shanghai World Financial Center both from free and ambient vibration response. Eng. Struct., 36, 14-26.

Stehly, L., Fry, B., Campillo, M., Shapiro, N.M., Guilbert, J., Boschi, L., Giardini, D., 2009. Tomography of the Alpine region from observations of seismic ambient noise. Geophys. J. Int., 178(1), 338-350.

Thompson, D., 2009. Railway Noise and Vibration. Mechanisms, Modelling and Means of Control. Elsevier, Oxford (GB).

Varone, C., Lenti, L., Martino, S., Semblat, J.F., Bozzano, F., 2019. Modelling of seismic urban wavefield in highly heterogeneous Site-City configurations, in Earthquake Geotechnical Engineering for Protection and Development of Environment and Constructions. Proceedings of the 7th International Conference on Earthquake Geotechnical Engineering, pp 5506-5512, eds Silvestri, F., Moraci, N., CRC Press/Balkema, Leiden (NL).

Varone, C., Lenti, L., Martino, S., Semblat, J.F., 2021. Spatial variability of the urban ground motion in a highly heterogeneous site-city configurations. Bull. Earthq. Eng., 19, 27-45.

Vella, A., Galea, P., D'Amico, S., 2013. Site frequency response characterisation of the Maltese islands based on ambient noise H/V ratios. Eng. Geol., 163, 89-100.

Wang, S., Sun, X., Liu, L., Zong, J., 2020. Sub-surface structures and site effects extracted from ambient noise in metropolitan Guangzhou, China. Eng. Geol., 268, 105526.

Washington, H.S., 1906. The Roman Comagmatic Region. Carnegie Institute, Washington (USA), publ n 57.

Wathelet, M., Chatelain, J.-L., Cornou, C., Di Giulio, G., Guillier, B., Ohrnberger, M., Savvaidis, A., 2020. Geopsy: a user-friendly open-source tool set for ambient vibration processing. Seismol. Res. Lett., 91(3), 1878-1889.

Xu, Q., Xiao, Z., Liu, T., Lou, P., Song, X., 2015. Comparison of 2D and 3D prediction models for environmental vibration induced by underground railway with two types of tracks. Comput. Geotech., 68, 169-183.

Yamanaka, H., Dravinski, M., Kagami, H., 1993. Continuous measurements of microtremors on sediments and basement in Los Angeles, California. Bull. Seismol. Soc. Am., 83(5), 1595-1609.

Yang, Y.B., Hsu, L.C., 2006. A review of researches on ground-borne vibrations due to moving trains via underground tunnels. Adv. Struct. Eng., 9(3), 377-392.

Yang, Y.B., Liang, X., Hung, H.H., Wu, Y., 2017. Comparative study of 2D and 2.5 D responses of long underground tunnels to moving train loads. Soil Dyn. Earthq. Eng., 97, 86-100.

Yaseri, A., Bazyar, M.H., Hataf, N., 2014. 3D coupled scaled boundary finite-element/finite-element analysis of ground vibrations induced by underground train movement. Comput. Geotech., 60, 1-8.

Yates, A.S., Savage, M.K., Jolly, A.D., Caudron, C., Hamling, I.J., 2019. Volcanic, coseismic, and seasonal changes detected at White Island (Whakaari) volcano, New Zealand, using seismic ambient noise. Geophys. Res. Lett., 46(1), 99-108.

Young, C.J., Chael, E.P., Withers, M.M., Aster, R.C., 1996. A comparison of the high-frequency (> 1 Hz) surface and subsurface noise environment at three sites in the United States. Bull. Seismol. Soc. Am., 86(5), 1516-1528.

Zhang, X., Zhou, S., He, C., Di, H., Si, J., 2021. Experimental investigation on train-induced vibration of the ground railway embankment and under-crossing subway tunnels. Transp. Geotech., 26, 100422.

Zhou, S., He, C., Di, H., Guo, P., Zhang, X., 2017. An efficient method for predicting train-induced vibrations from a tunnel in a poroelastic half-space. Eng. Anal. Bound. Elem., 85, 43-56.

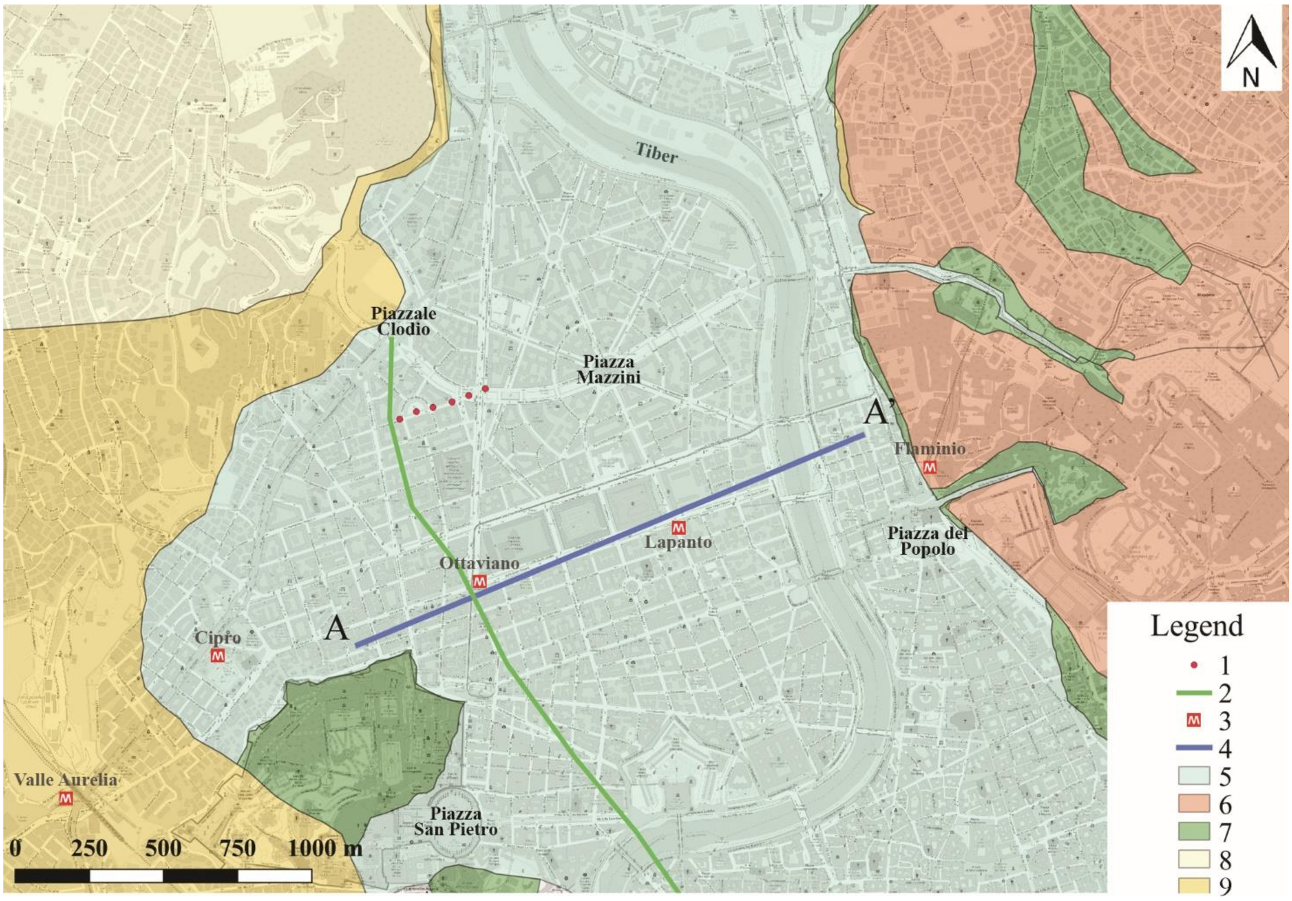

Figure 1. Geological map of the Prati neighbourhood with the location of the ambient vibration measurements; legend: 1) ambient vibration measurements; 2) line C designed path; 3) line A underground station; 4) geological cross-section A-A’ (Fig. 2); 5) Tiber River alluvial deposits (Pleistocene-Holocene); 6) volcanic deposits (Middle Pleistocene); 7) Pre-Würmian fluvio-palustrine deposits (Middle Pleistocene); 8) Monte Mario Formation (Lower Pleistocene); 9) Marne Vaticane Formation (Pliocene-Pleistocene).

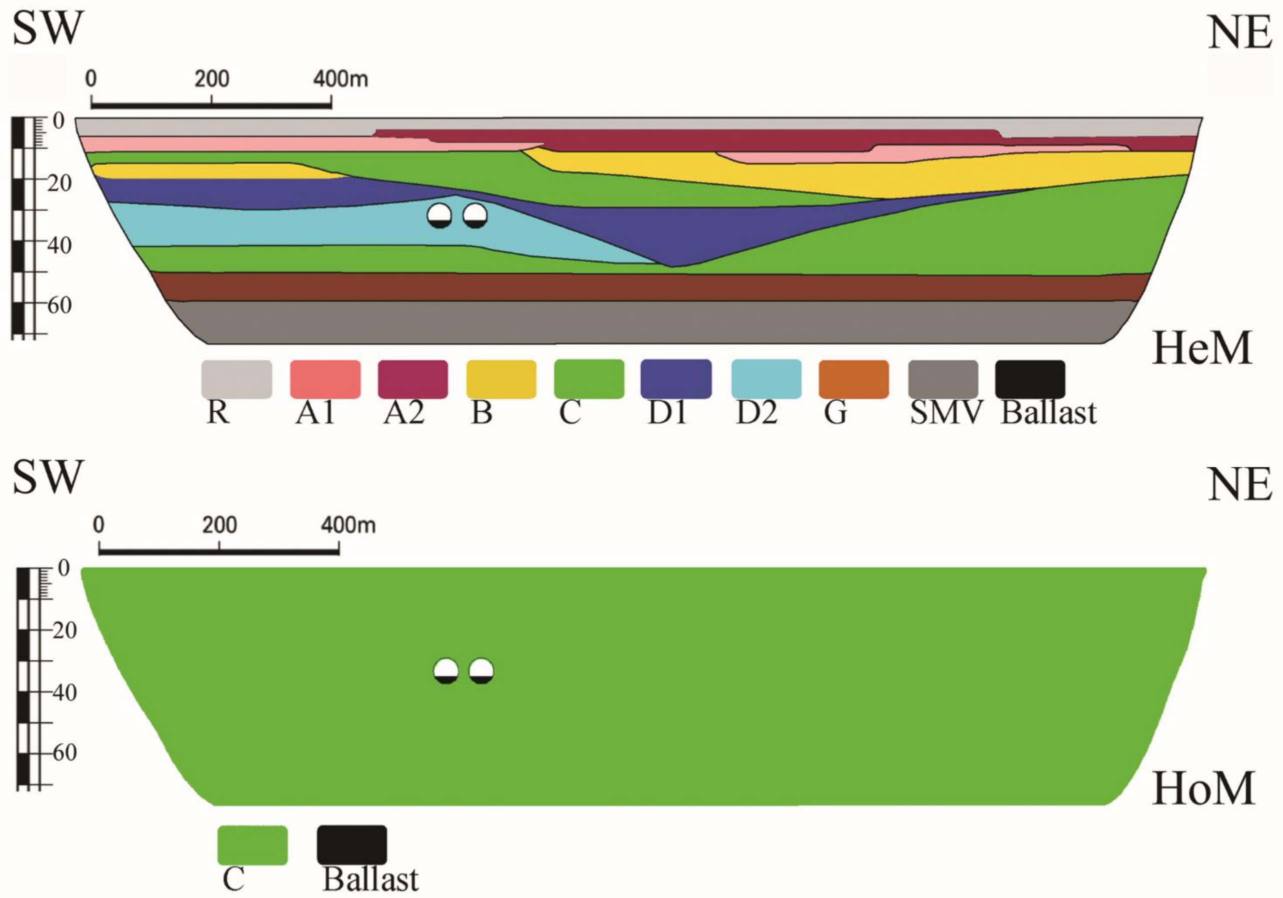

Figure 2. Engineering geological models for HeM (top) and HoM (bottom) along cross-section AA’ of Figure 1.

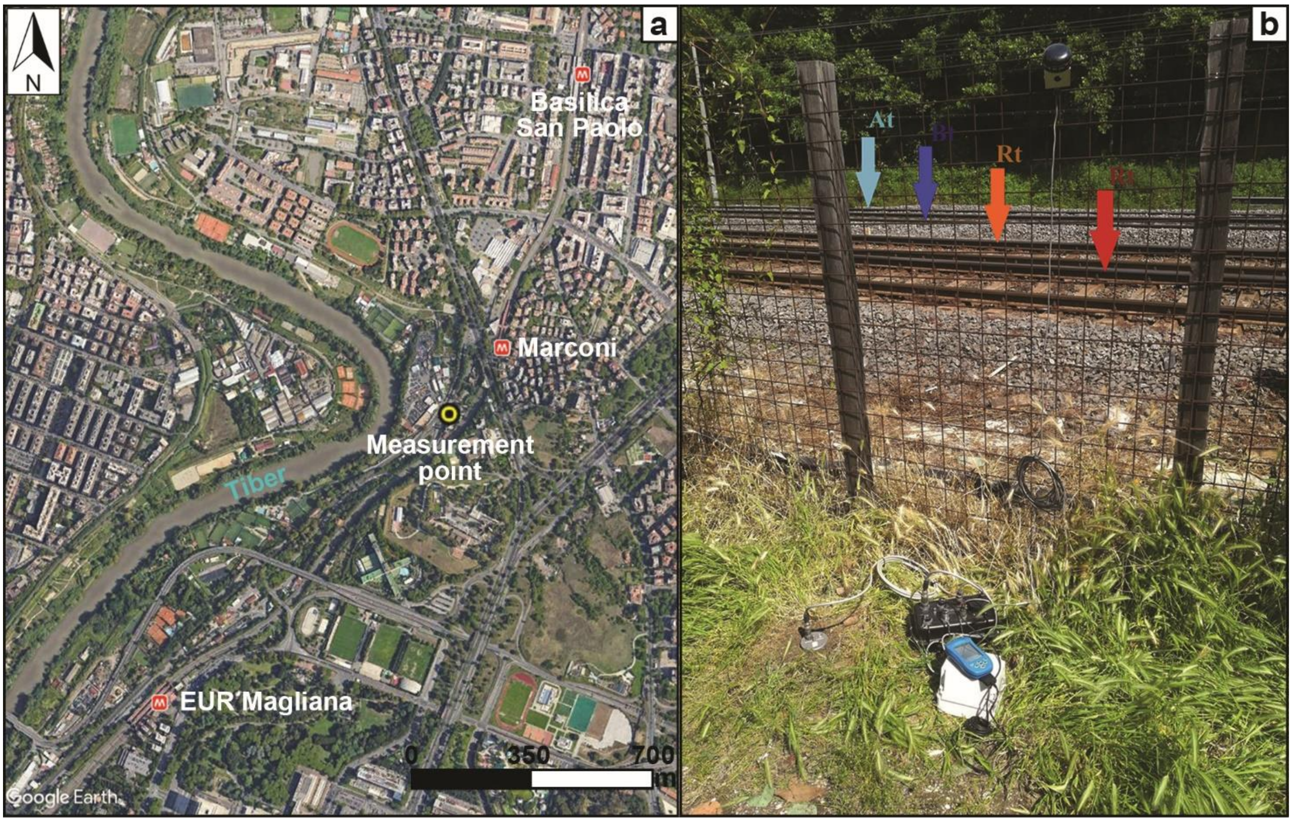

Figure 3. Measurement of vibrations due to train transit: a) satellite view of the measurement site (from Google Earth); b) photo view of the measurement configuration: LE-3Dlite MkIII three-component seismometer of Lennartz Electronic GmbH and REFTEK 130-01 datalogger; arrows indicate tracks of accelerating trains (At) and braking trains (Bt) of line B and tracks of regularly transiting trains (Rt) of the Roma-Lido line.

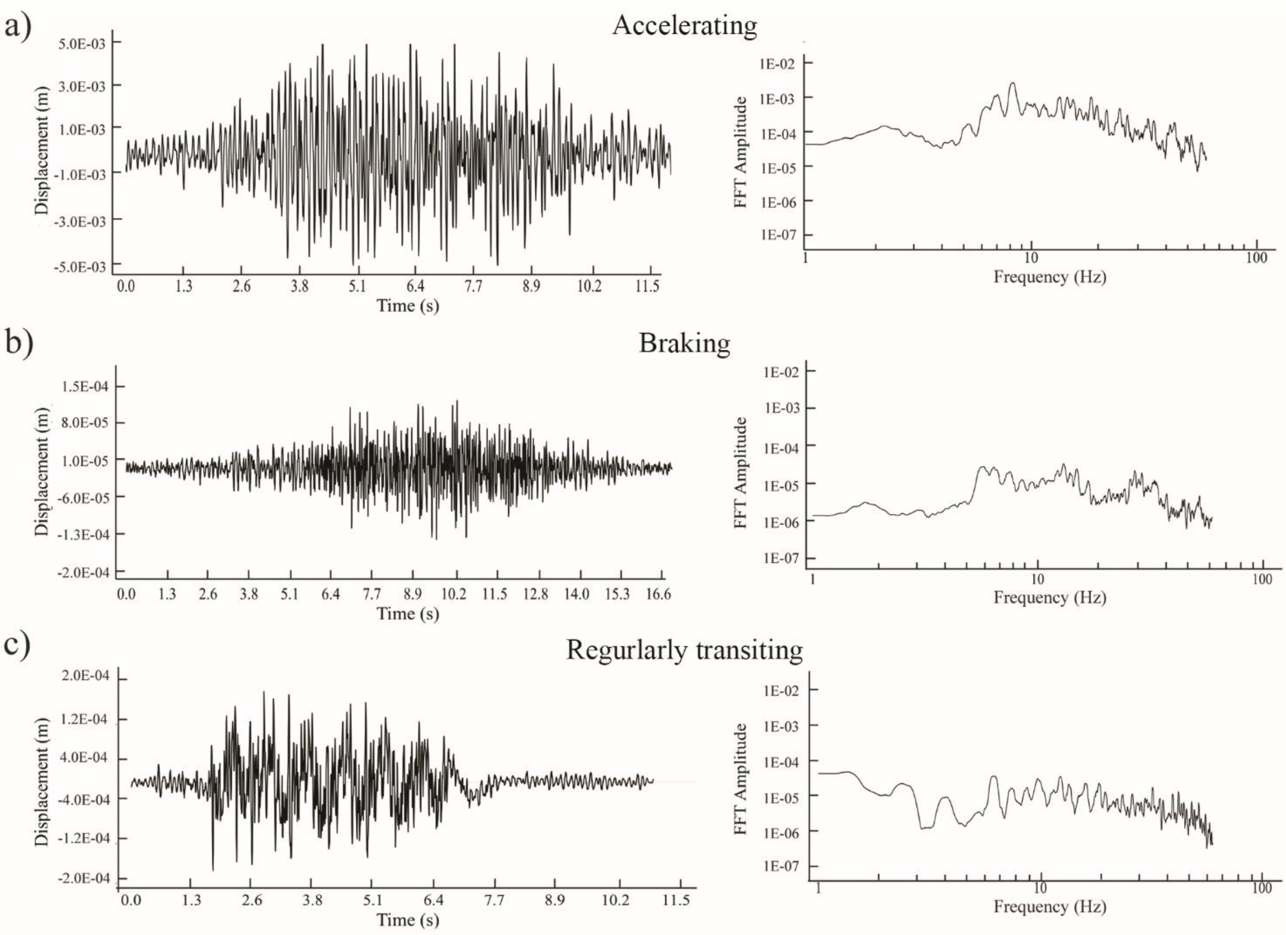

Figure 4. Time histories (left) and FFT spectra (right) for the selected accelerating (a), braking (b) and regularly transiting (c) trains.

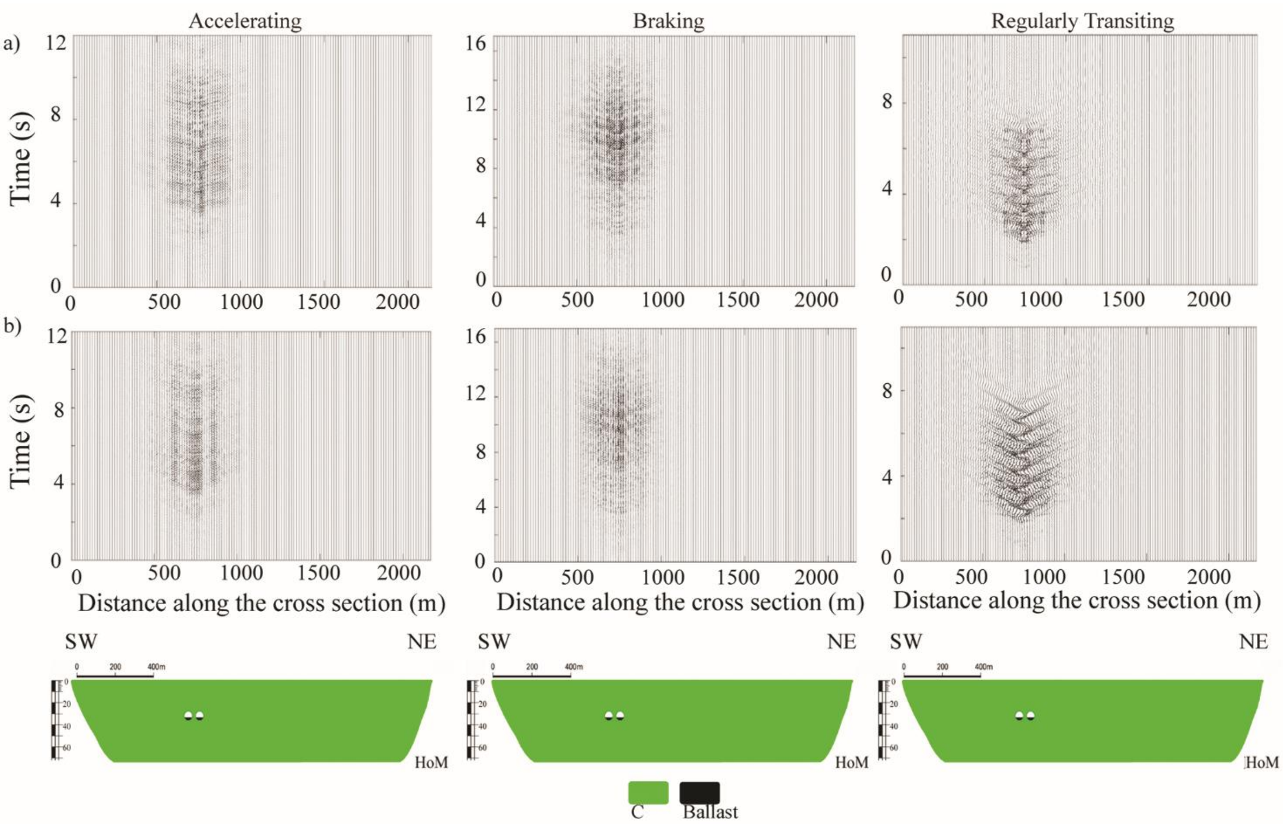

Figure 5. WPM showing horizontal (a) and vertical (b) displacement time histories along the HoM surface for accelerating (left), braking (centrum) and regularly transiting (right) trains; time history amplitude at the same scale for each train transit modelling.

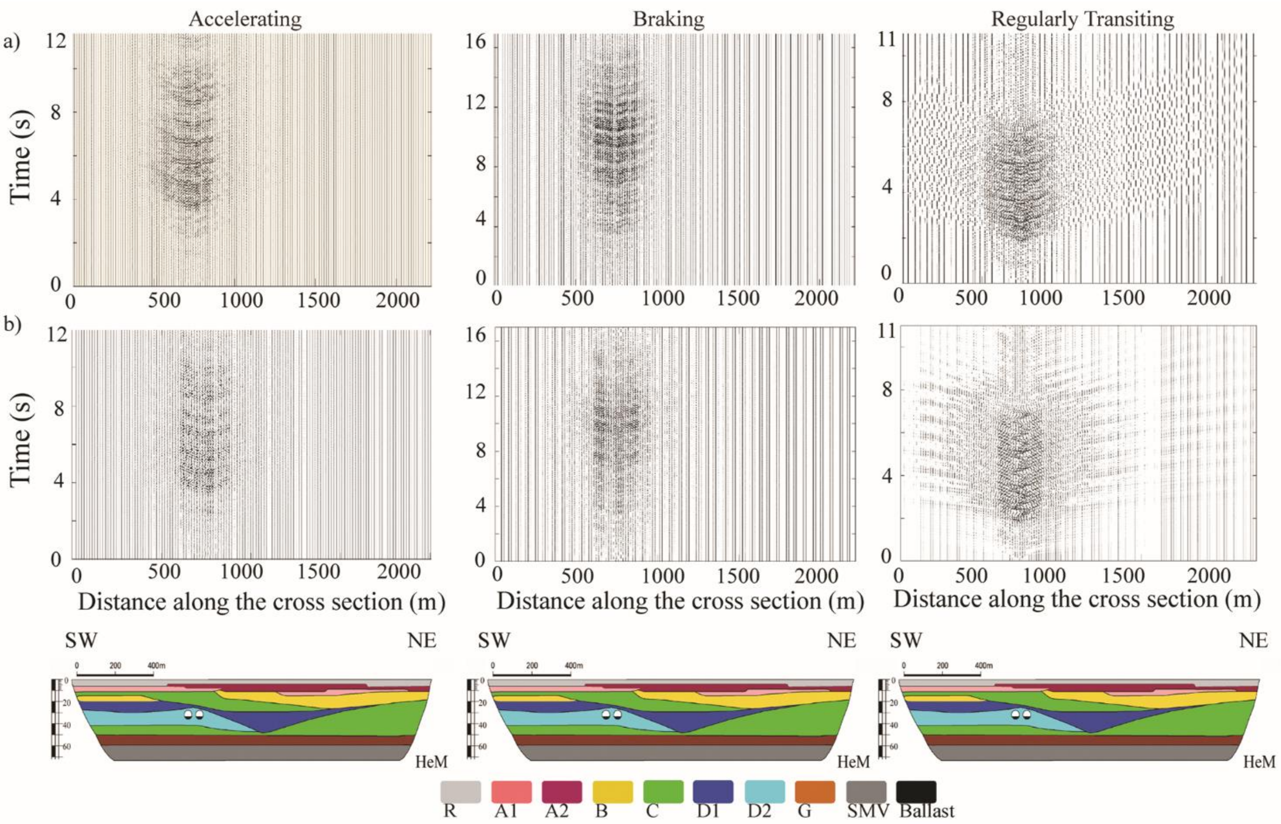

Figure 6. WPM showing horizontal (a) and vertical (b) displacement time histories along the HeM surface for accelerating (left), braking (centrum) and regularly transiting (right) trains; time history amplitude at the same scale for each train transit modelling.

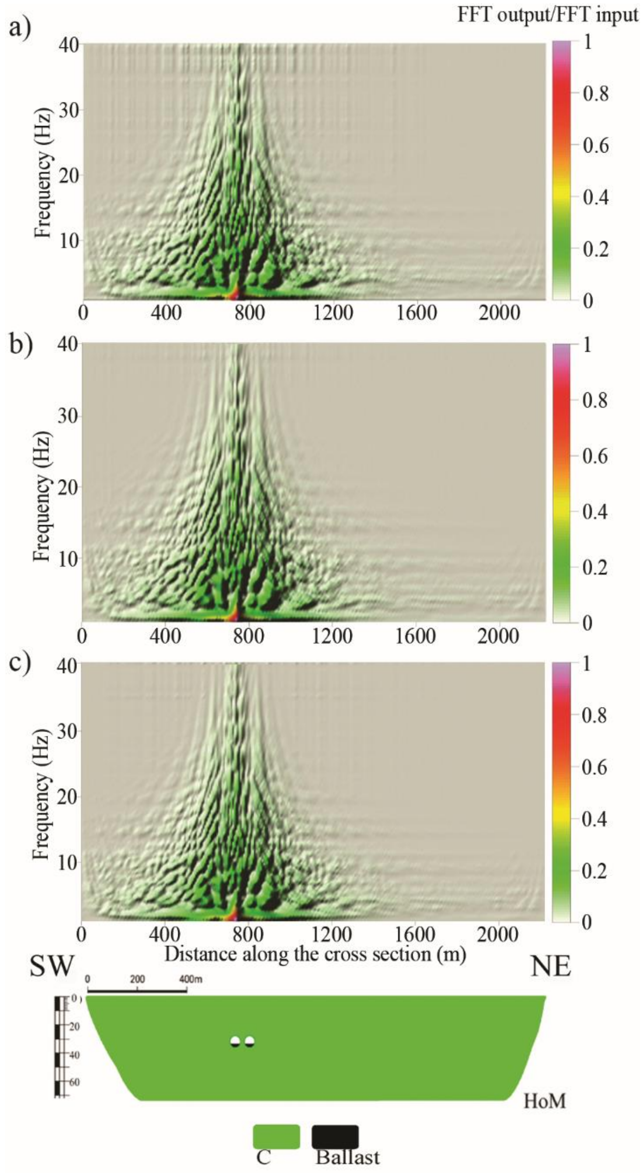

Figure 7. FFT spectral ratio between the ground motion at the free surface (output) and the applied input of train transit resulting for the HoM for accelerating (a), braking (b) and regularly transiting (c) trains.

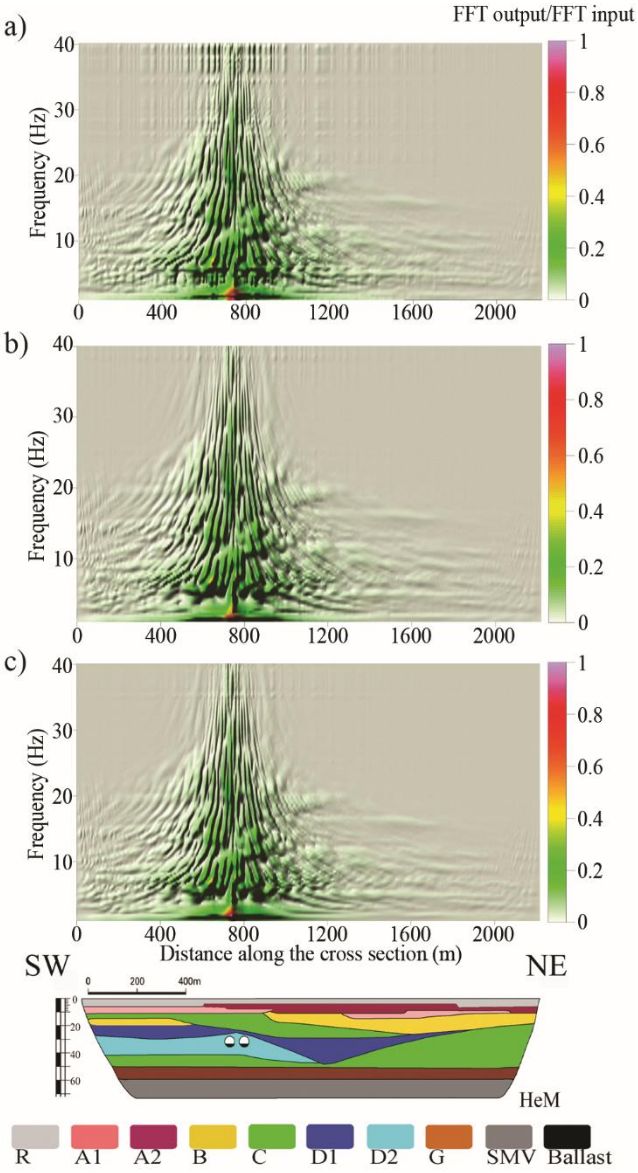

Figure 8. FFT spectral ratio between the ground motion at the free surface (output) and the applied input of train transit resulting for the HeM for accelerating (a), braking (b) and regularly transiting (c) trains.

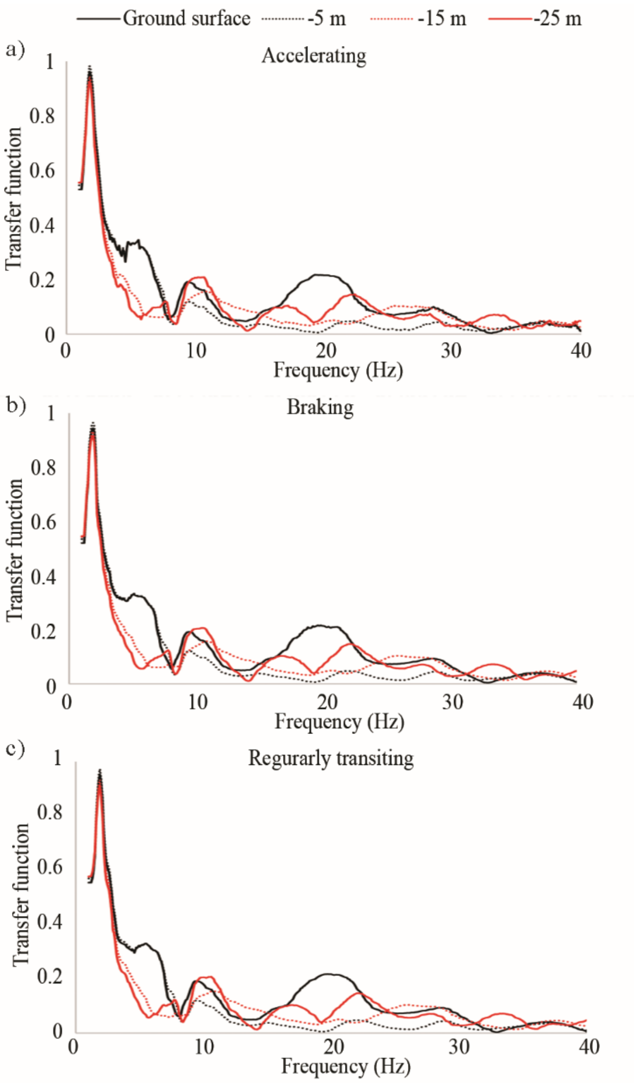

Figure 9. Transfer functions obtained at the ground surface and within the soil (-5 m, -15 m and -25 m of depth from the ground surface) for the HeM for accelerating (a), braking (b) and regularly transiting (c) trains.

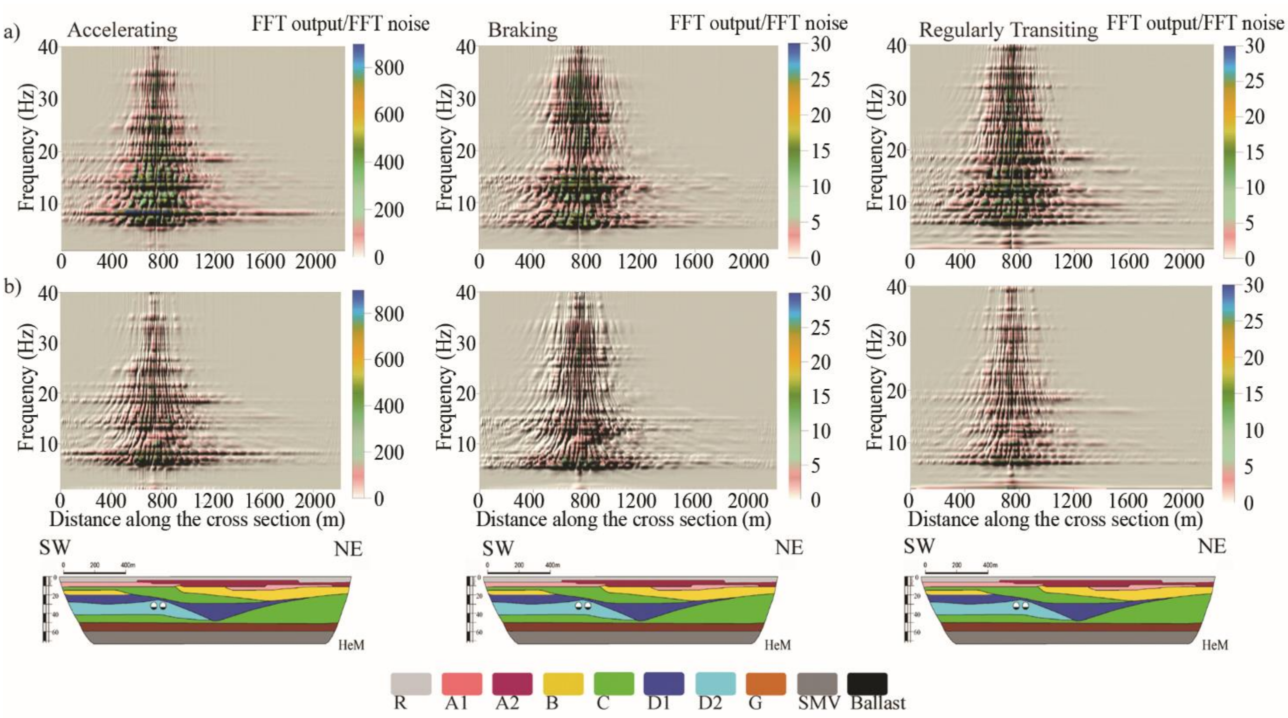

Figure 10. Distribution of vertical (a) and horizontal (b) FFT spectral ratios along the HeM cross-section between surface motion (output) and ambient vibration noise for accelerating (left), braking (middle) and regularly transiting (right) trains.

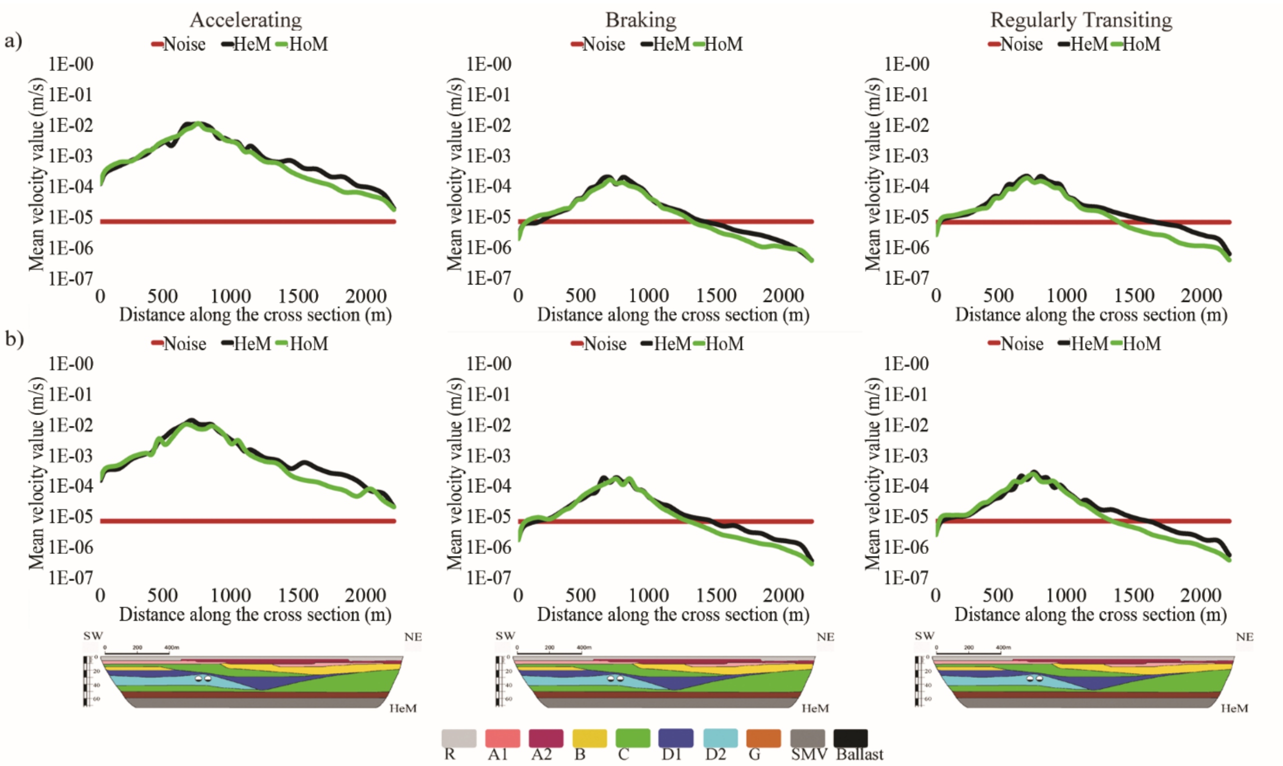

Figure 11. Distribution of vertical (a) and horizontal (b) mean velocities along cross-section AA’ in the HoM (green line) and HeM (black line) for the considered inputs: accelerating (left), braking (middle) and regularly transiting (right) trains.

Unit	**ρ** (kg/m³)	**ν**	**E** (MN/m²)	**ξ(%)** strain=0.001%	**Q**	**α**	**β**	**Vs** (m/s)
R	1800	0.3	217.0	5	10	2.2460	3.370E-04	220
A1	1875	0.3	262.5	6	8	2.6390	4.640E-04	239
A2	1875	0.3	262.5	6	8	2.6390	4.640E-04	239
B	1916	0.3	310.0	1	50	0.5655	9.950E-05	260
C	1865	0.3	210.0	3	17	1.6210	2.850E-04	212
D1	1957	0.3	835.0	3	17	1.6210	2.850E-04	417
D2	2057	0.3	252.5	6	8	2.6390	4.640E-04	417
G	2140	0.3	2670.0	1	50	0.5655	9.950E-05	713
SMV	2078	0.3	1152.5	3	17	1.6210	2.850E-04	461
MV	2078	0.3	4425.0	1	50	0.5655	9.950E-05	923
Ballast	2500	0.3	31780.0	3	17	1.6210	2.850E-04	2255

Table 1. Physical and mechanical parameter values attributed for the numerical modelling of the lithological units of the Tiber River valley; legend: ρ=density, ν=Poisson coefficient, E=Young modulus, ξ=damping ratio at strain 0.001(%), Q=mean damping quality factor, α and β=Rayleigh constants, Vs=S-wave velocity.